Research Square

Preprints are preliminary reports that have not undergone peer review.
They should not be considered conclusive, used to inform clinical practice,
or referenced by the media as validated information.

Human tubuloids from cryopreserved adult tissue: building a biobank for 3D modeling and precision medicine

Cindy Giraldo
Instituto Aragonés de Ciencias de la Salud
Alodia Lacueva-Aparicio
Instituto de Investigación Sanitaria Aragón
Rebeca Sanz-Pamplona
Instituto de Investigación Sanitaria Aragón
Ester Raigón-Gómez
Instituto de Investigación Sanitaria Aragón
Laura Martínez-Gimeno
Instituto Aragonés de Ciencias de la Salud
María Pilar Torcal
Instituto Aragonés de Ciencias de la Salud
Ignacio Giménez
Instituto Aragonés de Ciencias de la Salud
Ignacio Ochoa
Universidad de Zaragoza
Celia del Agua
Hospital Clínico Universitario Lozano Blesa
Paula Bermúdez-Javierre
Instituto Aragonés de Ciencias de la Salud
Izaskun Arenaz
Instituto Aragonés de Ciencias de la Salud
Irene Mora
Instituto Aragonés de Ciencias de la Salud
Purificación Catalina-Carmona
Biobanco del Sistema Sanitario Público de Andalucía
José Antonio Carrillo-Ávila
Biobanco del Sistema Sanitario Público de Andalucía
Carlos Hugo Mora Cevallos
Hospital Clínico Universitario Lozano Blesa
Jorge Subirá

Hospital Clínico Universitario Lozano Blesa

Delia Recalde-Frisón

Instituto Aragonés de Ciencias de la Salud

Teodora Ranđelović

Biomedical Research Networking Center in Bioengineering, Biomaterials and Nanomedicine

Mª del Mar Encabo-Berzosa

mmencabo.iacs@aragon.es

Instituto Aragonés de Ciencias de la Salud

Article

Keywords: organoids, biobank, kidney, tissue biopsy, NAMs

Posted Date: June 30th, 2026

DOI: https://doi.org/10.21203/rs.3.rs-10084577/v1

License: This work is licensed under a Creative Commons Attribution 4.0 International License.
Read Full License

Additional Declarations: No competing interests reported.

Abstract

Tubuloids offer a powerful tool for advancing renal research and improving patient care. To facilitate this, we have established a robust biobank of 40 adult human kidney organoids derived from fresh or frozen biopsies. These organoids exhibit diverse morphologies, distal and proximal tubules, closely resembling their tissue of origin. We have extensively characterized these organoids using a combination of techniques, including histological staining, immunofluorescence, gene expression analysis (qPCR and RNA-seq), and genetic profiling (STRs). This comprehensive characterization ensures the quality and reliability of the organoids for downstream applications. Molecular analysis revealed the expression of genes characteristic of various kidney cell types. Furthermore, we have successfully cultured these organoids within microfluidic chips, demonstrating their compatibility with advanced culture systems. This platform of well-characterized, living human kidney organoids from fresh and frozen tissues provides a valuable resource for a wide range of biomedical research, including drug screening, disease modeling, and personalized medicine.

1. Introduction

Biobanks serve as invaluable resources for medical research, making available to researchers high quality and ethically managed complex collections of biological materials along with their associated clinical data. These materials include a wide range of specimens, such as tissues, biological fluids, biomolecules, and more recently organoids. Under the expert guidance of professional biobankers, these repositories have significantly contributed to knowledge of diseases and the development of innovative treatments, contributing to the development of personalized medicine (1, 2). The ability to establish long-term organoid cultures from patient tissue samples has driven the creation of specialized Biobanks dedicated to their culture, characterization, conservation, and distribution (3–5). Several initiatives are currently underway with the aim of forming such structures. Among them, the "HUB Organoids" Biobank stands out as a pioneer, founded by the Hubrecht Institute, Utrecht University Medical Center, and the Royal Netherlands Academy of Arts and Sciences (KNAW) (6). Recently, the successful generation of organoids from cryopreserved tissue has opened the door to establishing living biobanks, which streamline and optimize resources for organoid derivation (7–10).

Organoids can be defined as three-dimensional in vitro structures composed of cells that self-organize and differentiate into functional cell types that recapitulate the structure and function of the organ from which they were derived (11). These models are currently a very promising alternative, facilitating compliance with the 3Rs principles and enabling personalized modelling, as well as their application for the analysis of precision medicine strategies (12). In this context, kidney organoids have emerged as powerful tools for modeling kidney biology, studying diseases, and developing new therapies (13). Most studies have focused on organoids derived from induced pluripotent stem cells (iPSCs) or immortalized cell lines (14–17). Also, Schutgens et al. developed a protocol for tubuloid generation, maintenance and conservation from adult kidney and urine (18). Moreover, a biobank of kidney organoids derived from childhood kidney cancers has been established (19) and demonstrates that organoids recapitulate

tissue heterogeneity and its utility for disease modelling for personalized medicine (18, 19). Hence, the establishment of organoid biobanks from both healthy renal tissue and tumor tissue is equally important for understanding kidney biology and disease.

The generation of patient-derived organoids from adult biopsy samples typically requires fresh, viable tissue, representing a major bottleneck that restricts scalability, standardization, and the effective use of biobanked specimens (20–23). For that reason, the present work focuses on developing a robust, standardized protocol to generate tubuloids from frozen biopsies. Our findings establish that cryopreserved tissue serves as an equivalent and reliable source for organoid production. Generating organoids for all patients undergoing surgical procedures would be neither cost-effective nor feasible. However, the cryopreservation of surgically resected tissues for subsequent organoid derivation, for instance, in the context of testing personalised medicine strategies, represents a highly valuable approach from both a scientific and clinical prespective, therefore we propose an efficient long-term conservation strategy that facilitates the creation of viable organoid models from frozen repositories. Obtained tubuloids were characterized using hematoxylin and eosin staining, immunohistochemistry, immunofluorescence, qPCR and transcriptomics data (RNA-seq). Tubuloids derived from multiple donors maintained their viability and functional integrity post-thawing, enabling the establishment of a biobank under rigorous ethical and quality control standards.

Establishing biobanks from cryopreserved tissue provides essential flexibility compared to the constraints of fresh samples. Here, we demonstrate the successful generation of human kidney organoids from frozen specimens, enabling the creation of a multifaceted organoid repository. These models maintain a dedifferentiated state, granting them high plasticity and making them an ideal substrate for studying differentiation into specific renal lineages. Moreover, we demonstrated the compatibility of tubuloids with organ-on-a-chip models, offering advanced systems for different applications.

2. Materials and Methods

2.1 Ethics statement

Sample collection was performed by using surplus diagnostic material provided by the Pathology Departments of participating hospitals (Hospital Clínico Universitario Lozano Blesa and Hospital Universitario Miguel Servet), within the framework of the Biobank of the Aragon Health System (National Registry of Biobanks, B.0000873), which is integrated into the ISCIII Platform for Biobanks and Biomodels (PT23/00146). All patients provided written informed consent in accordance with the Biobank's approved consent model, and all samples were pseudonymised to ensure patient confidentiality.

All methods were carried out in accordance with the relevant guidelines and regulations and in strict compliance with the principles of the Declaration of Helsinki.

This collection was developed following prior approval by the relevant Ethics and Scientific Committees, including the Aragon Clinical Research Ethics Committee (CEICA) (ref COL22-005).

The derived organoids form part of the Biobank's Organoid and Epithelioid Collection and are available to the research community, together with their associated clinical data, upon request (biobanco.iacs@aragon.es).

2.2 Human tissues

Freshly excised kidney samples from adult patients were dissected in the Hospital Pathological Anatomy laboratory, and a small part of the kidney cortex was selected. The tissue was maintained in Advanced F-12 medium (Gibco, 12634010) at 4°C until processing up to 72 h.

2.3 Tissue processing

For direct fresh tubuloid generation, tissue was minced into 5 x 5 mm under aseptic conditions. For tissue cryopreservation, specimens were sectioned into approximately 0.5 x 0.5 cm fragments under aseptic conditions within a biosafety cabinet. The tissue pieces were then snap-frozen in a cryopreservation medium consisting of FBS and DMSO (9:1). Vials were initially stored at -80°C before being transferred to liquid nitrogen (LN_2) for long-term storage.

2.4 Organoid Derivation

The selected fresh or frozen tissue was minced in ~ 1 mm^3 pieces and washed three times before digestion in 1 mg mL^{-1} collagenase solution (Sigma, C9407) and 10 µM Rho-kinase inhibitor Y-27632 (Abmole) during 45 min at 37°C shaking the tube in a thermoblock at 750 rpm. The digestion was stopped with Advanced F-12 medium, and the dilution was passed through a 100 µm micro-pored strainer to obtain an epithelial-enriched cell fraction and discard big tissue fragments. Next, the throughout was washed with Advanced F-12 medium and centrifuged at 300×g 5 min, RT. In case of a visible red pellet, erythrocytes were lysed in 1 mL red blood cell lysis buffer (Roche) for 5 min, RT, before the addition of 10 mL Advanced F-12 medium. Then, the samples were centrifuged at 300×g, 5 min, RT. Finally, the cell pellets were seeded in Cultrex growth factor-reduced BME-II (Biotechne) and cultured in kidney organoid complete medium (Advanced F-12 medium (Gibco) supplemented with N-acetilcysteine (1,25 mM, Sigma), B-27 supplement (1,5X, Gibco), R-spondin-3 conditioned medium (2X, Immunoprecise), EGF (50 ng mL-1, Peprotech), FGF-10 (100 ng mL-1), Rho-kinase inhibitor Y-27632 (10 µM, Abmole) and A83-01 (5 µM, Tocris Bioscience). Medium was renewed every 2–3 days and tubuloids were split (1:2 – 1:3) every 1–3 weeks.

2.5 Organoid cryopreservation

Tubuloids were cryopreserved 2–3 days post-passage to ensure an optimal size for post-thaw viability. For each cryovial (500 µL) the contents of 2–4 wells from a 24-well plate (MW24) were collected. The tubuloids were first incubated with dispase (1mg/mL; 5 µL per well) for 1 hour at 37°C to dissociate the extracellular matrix. The suspension was then transferred to a 15 mL conical tube and centrifuged at 300

xg for 5 minutes at room temperature (RT). After discarding the supernatant, the pellet was washed with 10 mL of basal medium and centrifuged again under the same conditions. The final pellet was resuspended in Recovery Cell Culture Freezing Medium (Gibco) and aliquoted into cryovials (500 µL). To ensure a controlled cooling rate, vials were placed in a CoolCell container and maintained at -80°C for 24–48 hours before being transferred to liquid nitrogen for long-term storage. For the recovery of cryopreserved tubuloids, vials were individually thawed in a 37°C water bath. The contents were then transferred to a 15 mL conical tube containing basal medium and centrifuged at 300 xg for 5 minutes at room temperature, RT. After carefully discarding the supernatant, the resulting pellet was resuspended in BME-II (40 µL per well). The organoid suspension was subsequently seeded into a pre-warmed 24-well plate and incubated at 37°C to allow for matrix gelation.

2.6 Kidney-on-a-chip model

Tubuloid-derived cells were obtained following the previously described protocol (Section 2.3). BME-II (Biotechne) coating was prepared from a stock solution of 10 mg/mL and diluted to a final concentration of 150 µg/mL. A total volume of 60 µL was added per channel in a six channel µ-Slide (µ-Slide VI, IBIDI, 80606) and incubated for 1 hour at room temperature. After incubation, the coating solution was removed by aspiration. Approximately 100,000 cells were seeded per channel of the microfluidic device. Once the channels reached confluence, cultures within the devices were maintained for seven days under bidirectional fluid flow performed in a rocker (IKA Rocker 2D Digital), with daily medium replacement.

2.7 Histochemistry (HC) and immunehistochemistry (IHC)

Tissues were fixed in a 4% neutral buffered formaldehyde solution, dehydrated and embedded in paraffin. Tubuloids were grown for one week in BME-II. After that time, the matrix was disrupted by incubating with dispase (0,1 mg ml^{-1}) for 1 hour. Once the matrix was eliminated, tubuloids were centrifuged at 300 xg, 5 min, RT and fixed in 4% neutral buffered formaldehyde solution for 30 min before washing 3 times with PBS, dehydrated and embedded in paraffin. Both tissues and organoid sections were subjected to H&E and immunohistochemical staining. Immunohistochemistry was performed according to standard protocols on 3 µm sections. The primary antibodies were Vimentin (RTU, Clone V9, Dako, Agilent) and Cytokeratin (AE1/AE3) (RTU, Clone AE1/AE3, Dako, Agilent) and the secondary antibody was EnVision FLEX, High Ph (Link) (K800021-2, Dako, Agilent). All images were scanned with an Axio Scan Z1 (Zeiss) in the Scientific and Technical Service of Pathological Anatomy at Aragon Institute of Health Science (IACS).

2.8 Immunofluorescence (IF)

Immunofluorescence was performed with a previously optimized protocol on 3 µm paraffin sections. After rehydration, antigen retrieval was performed using PT Link (Dako) at 95°C for 20 min in a low pH buffer (Dako antigen retrieval, low pH). Sections were then permeabilized for 1.5 hours, followed by two 5-minute washes. Next, they were blocked with 0.05% Triton X-100 and 1% BSA in PBS for 2 hours at room temperature. Primary antibodies were incubated overnight at 4°C in a humidity chamber, followed

by three 5-minute washes. Secondary antibodies were incubated for 2 hours at room temperature, followed by two 5 minutes washes. DAPI (Molecular Probes D3571) was used for nucleus counterstains. Finally, sections were cleaned and mounted with Fluoromout G (Invitrogen).

The antibodies were Lotus Tetragonolobus Lectinbiotinilated (LTL, 1:200, Vector), Uromodulin (UMOD,1:1000, Atlas Antibody HPA054721), protein zonula occludens (ZO-1,1:100, Invitrogen 40-2200), α tubulin (1:100, sc-23958), Streptavidin DyeLight 488 (1:40, Vector), goat anti-rabbit-Alexa 568 (1:500, Invitrogen A11036) goat anti mouse-Alexa 568 (1:500, Invitrogen A11031) and goat anti rabbit-Alexa 488 (1:500, Invitrogen A11034). Confocal images were taken with a ZEISS LSM 880 confocal microscope in the Scientific and Technical Service of Microscopy and Imaging at Aragon Institute of Health Science (IACS).

In the kidney-on-chip model, cells were fixed by 4% paraformaldehyde for 30 minutes, permeabilized with 0.2% Triton X-100 in PBS for 20 minutes and blocked with 3% BSA in PBS for 2 hours. Cells were incubated with antibodies against α tubulin (1:200 dilution, sc-23958), tight junction protein zonula occludens (ZO-1, 1:200, Invitrogen 40-2200), LTL biotinylated (1:200, Vector) overnight at room temperature in an orbital shaker, followed by incubation with anti-rabbit-Alexa 488 (1:500, Invitrogen A11070), anti-mouse-Alexa 555 (1:500, Invitrogen A28180) and Streptavidin DyLight 488 (1:40, Vector) for 1 hour. Finally, Hoechst nuclei staining (1:1000, Invitrogen 33342) was added and incubated for 20 minutes. Confocal images were taken with a Leica confocal microscope (STELLARIS DMi8, Leica).

2.9 STRs analysis

2.9.1 DNA Extraction and Quantification

For DNA extraction, 180 µL of ATL buffer were added to the tubuloids together with a stainless-steel bead (Qiagen, Ref. 69989) in a 2 mL tube. Tissue disruption was performed using a TissueLyser (Qiagen) by shaking for 2 minutes at 3500 rpm. Genomic DNA was subsequently purified using the DNA Blood and Tissue Kit (Qiagen, Ref. 69506), following the manufacturer’s instructions. DNA concentration and purity (A260/A280 and A260/A230 ratios) were assessed by spectrophotometry using a NanoDrop Ultra instrument.

2.9.2 STRs Analysis for Organoid Identification and Authentication

One nanogram of genomic DNA was used to perform a comprehensive analysis of 16 short tandem repeat (STRs) markers for organoid identification and traceability, in accordance with the standard recommendations for cell line authentication (ASN-0002-2022). This technique is based on PCR amplification of microsatellite regions (STRs markers), in which the number of repeat units varies between alleles at each locus, enabling unambiguous identification of cell lines and other biological samples.

STRs amplification was carried out using the AmpFlSTR Identifiler Plus PCR Amplification Kit (Applied Biosystems, Ref. 147624). The primer set included in the kit allows amplification of the following STRs loci: D8S1179, D21S11, D5S818, D7S820, CSF1PO, D3S1358, TH01, D13S317, D16S539, D2S1338, D19S433, vWA, TPOX, FGA, D18S51, and Amelogenin (sex marker).

Amplified STRs products were analyzed by capillary electrophoresis using a SeqStudio Genetic Analyzer (Applied Biosystems) equipped with a SeqStudio Genetic Analyzer Cartridge v2 (Applied Biosystems, Ref. A41331). STRs profiles were subsequently analyzed using GeneMapper ID-X software.

2.10 RNA extraction

RNA was extracted from frozen tissue samples and tubuloids using the miRNeasy Kit (Qiagen) according to the manufacturer's instructions. For tissue samples, 5 cuts of 20 µm were dissolved in Qiazol Lysis Reagent (Qiagen). Organoid RNA was extracted from cultures between passages 2 and 6, specifically after seven days in culture. Prior to RNA extraction, tubuloids were dissociated using dispase, centrifuged at 300 xg for 5 minutes at room temperature, and the resulting pellet was immediately snap-frozen. The frozen organoid pellet was then resuspended in Qiazol Lysis Reagent before proceeding with the miRNeasy protocol. RNA concentration and integrity were assessed using a Qubit fluorometer and RQI measurement, respectively. When possible, 250 ng of RNA were reverse transcribed to cDNA using the PrimeScript RT Master Mix Kit (Takara) according to the manufacturer's instructions.

2.11 Bulk RNA sequencing and analysis

A total of 16 samples (8 kidney tissues and 8 patient-derived tubuloids) from 5 different patients, including healthy and tumoral tissue, were profiled by RNA sequencing (RNAseq). Among the total, a subset of 16 samples corresponded to paired specimens from the same patients. After rRNA removal and library preparation, paired-end sequencing (150pb) was performed in Illumina NovaSeq X Plus Series.

Then, RNA-seq data were processed using a standardized pipeline. The quality of the raw reads was assessed using FastQC. Adapters and low-quality bases were trimmed using BBDuck tool. Then, reads were aligned to the GRCh38 using STAR. Gene annotation was performed using counts and transcripts per million (TPM) expression values were used for downstream analyses.

Principal component analysis (PCA) was performed to assess the major sources of variation in the gene expression dataset. PCA was computed on log2-transformed TPM expression values using the R function prcomp. The first two principal components were used to visualize sample clustering according to model type and sample type.

Differential gene expression (DGE) analysis was performed to identify genes differentially expressed between paired tissue and organoid samples (n = 16). Count expression data were analysed using linear modelling implemented in the *limma* (version 3.60.6) and *edgeR* (version 4.2.2) packages, with *voom*

transformation applied prior to contrast testing. To account for inter-patient variability, patient identity was included as a covariate factor in the model, allowing the analysis to focus on expression differences due to sample type. The criteria established for defining differentially expressed genes were set up with |log2 fold change| > 1 and adjusted p-value < 0.05.

Differential gene expression (DGE) analysis was performed to identify genes differentially expressed between paired tissue and organoid samples (n = 16). Count expression data were analyzed using negative binomial generalized linear models implemented in the DESeq2 package (version 1.44.0). To control for inter-patient variability, patient identity was included as a covariate in the design formula for paired comparisons (normal tubuloids vs tissues and tumoral tubuloids vs tissues). For unpaired comparison (fresh vs frozen-derived tubuloids), the model included sample type as the single explanatory variable. The criteria established for defining differentially expressed genes (DEGs) were set up with |log2 fold change| > 1 and a False Discovery Rate (FDR) < 0.05.

To estimate the relative enrichment of cell populations across samples, a gene set variation analysis (GSVA) was conducted using R package GSVA (version 1.52.3). Cell type–specific gene signatures were curated from previously published studies(18, 24, 25) (Supplementary Table 1). GSVA scores were subsequently scaled to z-score and visualized as a heatmap. Hierarchical clustering was performed using Euclidean distance and Ward's minimum variance method (Ward.D2). Statistical analyses were performed in R. Comparisons between paired normal tissue and tubuloid samples were conducted using two-tailed paired Student's t-tests and statistical significance was defined as $p < 0.05$. For the differentially significant co-expressed genes we performed gene enrichment with the enrichR package (version 3.4) to access the Enrichr platform (26–28) using MSigDB Hallmark Pathways. The pathways were arranged by adjusted p-value, and $p < 0.05$ was considered significant.

2.12 qPCR

QPCR was performed in tubuloids and kidney-on-chip model after seven days in culture once a complete monolayer was formed in the microfluidic device. Total RNA was reverse-transcribed into cDNA as previously described for RNA-seq samples. The relative abundance of specific gene transcripts was quantified by qPCR using the PreMix ExTaq (Probe qPCR) kit (TaKaRa Biotech, Dalian, China) on a QS7 thermocycler at the Genomics Service of the University of Zaragoza, Spain. mRNA levels of the target genes were normalized to RPLP0. Once the data on the cycles were obtained, the different conditions were analyzed with the 2ddCt analysis method. All primer sequences ara commercially available (IDT) and are summarized in Supplementary Table 2. The data obtained were analyzed statistically with GraphPad Prism 6 software. The graphs show the mean with its standard deviation (SD). The statistical test used for the analysis of qPCR results was multiple t-tests. Statistical significance was determined using the Holm-Sidak method, with alpha = 5.000%.

3. Results

3.1. Clinical sample characterization

In this study, 40 renal tubuloids from 22 different patients were successfully generated. Briefly, healthy renal tubuloids were derived from 22 distinct patient samples, with 91% success (22/24). Ten cases utilized fresh tissue as the starting material, while twelve were derived from frozen tissue stored between one month and three years. Furthermore, tumor-associated renal tubuloids were successfully derived from 18 patients, resulting in the establishment of paired healthy and tumoral tubuloids from 18 cases. The clinical data and sample characteristics were summarized in Supplementary Table 3. In the cohort of 22 patients (17 males, 5 females) the mean age at the diagnosis time was 63.31 ± 12.38 years. Males presented a slightly higher mean age (62.94 ± 11.58 years) compared to females (64.6 ± 16.33 years). Histologically, a variety of renal cell carcinomas were identified, with Clear cell renal cell carcinoma (ccRCC) being the most prevalent (17 cases). Less common subtypes included oncocytoma (2), Chromophobe renal cell carcinoma (chRCC) (1) and Xp11 translocation-associated renal cell carcinoma (tRCC) (2).

3.2. Establishment and characterization of tubuloids

To investigate the utility of complex cellular models, several lines of healthy and tumorigenic tubuloids were established. Those tubuloids generated from healthy tissue exhibited structures closely resembling those observed in the tissue of origin, including both proximal and distal tubules (Fig. 1A, B). Likewise, the paired tumor-derived samples recapitulated the cellular morphology of the original tumoral, corresponding to clear cell renal cell carcinoma (Fig. 1C, D). The epithelial nature of the cells was confirmed by positive staining for cytokeratin AE1/AE3 (Supplementary Fig. 1). High vimentin positivity in tubuloids suggested epithelial-mesenchymal transition and dedifferentiation of tubular cells, since in adult tissue vimentin is mainly expressed in glomerular podocytes and endothelial cells (Supplementary Fig. 1). Immunofluorescence staining was performed to confirm the presence of specific markers from renal tissue in the tubuloids derived from healthy renal tissue. Proximal tubules were identified by LTL immunostaining, and UMOD was used as a marker for the thick ascending limb of Henle's loop (Fig. 2C). These proteins were highly present in healthy tissue, but their expression in tubuloids was heterogeneous and only some of the tubuloids showed positivity (Fig. 2D). While podocin was present in the original tissue, its absence in the tubuloids suggests they primarily recapitulate tubular segments rather than mature glomeruli (data not shown).

Genetic identification of tubuloids generated from 9 normal and 3 tumoral tissue was carried out by analyzing 16 STR fragments. The correspondence of all the STR markers analyzed was 100% between the tubuloids and the samples from which they were generated (Supplementary Table 4).

3.3. Transcriptomics analysis

To characterize the differentiation state of the generated models, RNA sequencing was performed on tissues of origin and tubuloids derived from both fresh and frozen tissue, including healthy and tumor regions. Principal Component Analysis (PCA) (Supplementary Fig. 3) revealed distinct transcriptomic signatures: PC1 (accounting for 48.5% of total variance) clearly separates tubuloids and tissues, as expected. Interestingly, PC2 (16.6% of total variance) separates normal from tumoral tissues and two out

of three normal from tumoral tubuloids. Healthy tissues and tumor tissues each formed independent clusters. This is not as clear in the case of tubuloids. Moreover, tumor-derived organoids exhibited higher dispersion, probably reflecting their inherent interpatient heterogeneity.

Our data demonstrate that while tubuloids derived from normal tissue maintained core epithelial markers, they were significantly enriched in progenitor cell signatures. The expression of specialized cell-type markers was reduced, indicating a regenerative, dedifferentiated state compared to native tissue. However, these markers remained detectable, confirming the adult-derived nature of the models, and supporting the immunofluorescence results shown before (Fig. 3A).

Functional enrichment analysis identified a significant upregulation of stress-response pathways (e.g., TNF-alpha Signaling via NF-kB, hypoxia) and proliferation-related gene sets (E2F targets, G2-M checkpoint, mitotic spindle), compared to the tissue of origin, consistent with a regenerative phenotype of tubuloids (Fig. 3B). Furthermore, a clear metabolic adaptation was observed, characterized by the upregulation of glycolysis and cholesterol homeostasis alongside the downregulation of oxidative phosphorylation and fatty acid metabolism. Notably, xenobiotic metabolism was significantly downregulated, reflecting the observed loss of key specialized transporters (Fig. 3B).

Comparison of tumoral tubuloids with their native tissue showed a downregulation of genes associated with endothelial and immune cells, demonstrating the loss of non-tumoral components of tumor microenvironment. Similar to healthy organoids, proliferation, epithelial-mesenchymal transition and metabolic reprogramming were upregulated compared to the tissue of origin.

Next, to validate differences between tubuloids derived from fresh and frozen normal tissues, we compared their expression profiles. Even though sample number was low, with three fresh and two frozen samples, our results suggest that tubuloids derived from frozen tissue may be more mature than tubuloids derived from fresh tissue. Genes upregulated in fresh-derived tubuloids were primarily associated with kidney repair and proliferation, such as TNC, CSF1, TNFAIP2, SRPX2, all activated after renal injury and promoting proinflammatory signaling (29–31). Conversely, several of the most significant genes upregulated in frozen-derived tubuloids are critical for renal physiology, including transporters and enzymes such as SLC14A2 (urea transporter), SLCO4C1 (organic anion transporting polypeptide), SLC22A6 (OAT1), BBOX1 (carnitine synthesis), and (Fig. 3C).

3.4. Kidney-on-chip model based on patient-derived tubuloids

Once tubuloids were characterized, the next step was to generate a kidney-on-chip model to have a complete and polarized cell monolayer towards the lumen of the microfluidic device. Healthy tubuloids from two different donors were seeded in microfluidic devices and they generated a complete monolayer in up to seven days. The morphology and cellular organisation was highly heterogeneous throughout the monolayer, with cells displaying both polyhedral and fusiform morphologies in all samples analyzed. Zonula occludens-1 (ZO-1), a tight junction protein in epithelial cells, was used to evaluate cell–cell

junction formation and delineate cell boundaries. In addition, α-tubulin was also used to visualize the cytoskeleton and the primary cilium to assess cell polarization, as its apical localization indicates polarization toward the tubular lumen (Fig. 4). The specific marker LTL was also utilized, confirming its presence through different passages but not throughout all monolayer or even all samples analyzed (Supplementary Fig. 3). This findings confirmed RNAseq results where LTL and showed low expression in kidney tubuloids.

qPCR analysis was performed to compare kidney organoids cultured under standard conditions with tubuloids seeded in microfluidic devices (Fig. 4D,E). No significant differences were observed between both conditions for most of the analyzed markers. These results further confirmed the RNA-seq data, which showed a complete loss of expression of several transporters, including SLC22A6 (OAT1), SLC22A8 (OAT3), SLC22A1 (OCT1), and SLC5A2 (SGLT2). In contrast, the expression of other markers, such as AQP1, SLC12A3 (NCC), SLC12A2 (NKCC1), and SLC12A1 (NKCC2), as well as developmental genes including PROM1, PAX8, and SOX9, was maintained. The only marker showing a significant difference between organoids and kidney-on-chip cultures was PRKAA1 (AMPKα1) (Fig. 4D).

4. Discussion

Given the increasing need to recapitulate complex tissue structure and function, New Approach Methodologies (NAMs)—such as kidney organoids and organ-on-a-chip models—have emerged as the future gold standard for in vitro modeling(32–34). For these advanced applications, tissue biobanks have positioned themselves as essential providers of high-quality samples and associated clinical data (35, 36).

Kidney organoids can be derived from pluripotent stem cells (PSCs) or adult stem cells (ASCs). Organoids derived from PSCs represent fetal kidneys, making them primarily useful for studies in kidney development, fetal nephrotoxicity and regenerative medicine. ASC-derived organoids, generated from patient tissue, primarily mimic adult kidney tubular epithelium (hence tubuloids), and are useful for disease modelling, drug screening and nephrotoxicity testing (13).

Most tubuloids are generated from fresh tissue shortly after extraction (18, 24, 37, 38). Although some gastrointestinal, lung, breast and skin cancer organoids have been derived from frozen tissue (4, 7, 10, 39, 40), only a couple of studies have successfully established tubuloids from frozen tissue fragments (10, 39). In this work, we established a robust biobank comprising tubuloids from both healthy and tumoral adult tissues using fresh and frozen patient samples. To our knowledge, this is the most extensive biobank of kidney derived organoids from frozen tissue. Our described protocol to obtain viable tubuloids from long-term cryopreserved tissues clearly simplifies the previously described methods (7, 10), reducing the tissue manipulation before cryopreservation.

By implementing a modified version of the protocol described by Schutgens et al. (18), we successfully generated tubuloids that faithfully recapitulate the morphologic and phenotypic characteristics of the original primary epithelial tissue. Notably, the healthy organoid lines encompass functional epithelial

cells representing the majority of nephron segments, spanning from the proximal to the distal tubules. This morphological heterogeneity provides a significant advantage over homogeneous cultures, as it more closely recapitulates the complex architecture of the human kidney, thereby enabling more in-depth physiological studies. However, as shown in literature, tubuloids have a regenerative phenotype, exhibiting an increase in stemness and dedifferentiation markers and decrease in expression of kidney-specific transporters and a downregulation of xenobiotic metabolism. The regenerative state of tubuloids enables prolonged cell culture and the expansion of precious patient tissue, but it promotes metabolic changes towards glycolysis instead of oxidative phosphorylation due to nutrient-rich media and high proliferation rates (13, 18).

Our findings indicate that tubuloids generated from cryopreserved tissues show a more mature phenotype. Processing fresh tissue seems to enhance the regenerative phenotype of epithelial cells, as they attempt to repair the kidney following the invasive extraction procedure (41, 42). On the contrary, tubuloids derived from frozen tissue showed higher expression of kidney-specific transporters, maintaining certain mature functional traits of the kidney more effectively. These findings imply that cryopreservation could support the survival of more robust, differentiated epithelial cells, or potentially impact highly proliferative, injury-responsive stem cells that are active in fresh tissue. Even though it is not known how freezing can affect kidney tissue, it was shown that cryopreservation method could affect different structures of kidney organoids (43). However, frozen-derived tubuloids still maintain dedifferentiated regenerative phenotype. For better understanding of kidney physiology, as well as for drug screening and nephrotoxicity studies, more mature advanced models are needed. This could be achieved by co-culturing with other cell types, controlling molecular signaling, applying mechanical stimulation or promoting metabolic reprogramming(44).

The main source for the generation of renal organoids has been induced pluripotent stem cells (iPSCs) (14, 16, 45–49), and these organoids have also been employed in organ-on-a-chip models (50–52). However, differentiation protocols toward renal cell types remain labor-intensive, time-consuming, and costly. Therefore, the establishment of a biobank containing organoids derived from adult renal tissue provides researchers with rapid and accessible access to these samples within a relatively short timeframe. Kidney-on-a-chip platforms effectively replicate the dynamic microenvironmental stimuli critical for in vivo renal function. These systems enable the strategic seeding of tubuloids within chambers that mimic the nephron, allowing for the application of controlled laminar flow and mechanical stress. Perfusion within the chip promotes the maturation and polarization of tubular epithelia, enhances vascular differentiation, and, crucially, sustains barrier and reabsorption functions over extended periods. Synergizing these strategies provides a powerful tool for developing physiologically relevant in vitro models, bridging the gap in personalized medicine and drug discovery (54). To our knowledge, few studies (18, 44, 55–57) have explored the integration of adult kidney organoids into organ-on-a-chip (OoC) platforms. By utilizing our kidney organoid biobank, we aim to expand upon these findings. Specifically, we have successfully cultured tubuloids from two different patients across multiple passages, comparing traditional matrix-based protocols with chip-based environments. Results from the comparison between tubuloids and the kidney-on-chip model by qPCR showed that the differential

expression of AMPKα1 may reflect metabolic adaptations induced by differences in oxygen and nutrient gradients and shear stress, which are known to influence cellular energy-sensing pathways. No further statistically significant differences were observed. Therefore, our results demonstrate that, without maturation stimuli, this biomimetic model preserves the same phenotypic expression and morphological characteristics as those grown in standard matrix cultures. This shows the potential of our model for further differentiation and maturation of different tubular parts, with the advantage of accessibility of the apical epithelial side for stimuli application, drug screening and infection assays.

In conclusion, the establishment of a renal organoid biobank derived from cryopreserved tissue offers a highly accessible and flexible platform for personalized medicine, providing associated clinical data and standard quality procedures. By successfully generating paired tumoral and healthy tubuloids from frozen specimens, we provide a consistent source of standardized, dedifferentiated material characterized by high plasticity. This unique undifferentiated state facilitates directed differentiation into diverse renal lineages, making these tubuloids an ideal substrate for integration into kidney-on-a-chip systems. Ultimately, this synergy between cryopreserved biobanking and microfluidic technology paves the way for sophisticated *in vitro* models essential for advanced drug screening and toxicity studies.

Declarations

Funding

This work was supported by the Spanish Ministry of Science and Innovation (MICIN) and the National Biobanks and Biomodels Platform of the Instituto de Salud Carlos III (ISCIII) [Grant No. PT23/00146 and Grant No. PT23/00186].

Author Contribution

C.G. and A.L.-A. contributed equally to this work. M.M.E.-B. and T.R. contributed equally as senior authors. C.G. and M.M.E.-B. generated, characterized, and performed all organoid experiments. L.M.-G., M.P.T., and I.G. performed PCR analyses. C.A. carried out the anatomopathological evaluation. I.A., I.M., P.B.-J., and D.R.-F. collected and processed samples. P.C.-C. and J.A.C. performed and analyzed STR assays. J.S. and C.H.M.C. contributed to clinical data and patient recruitment. I.O., T.R. and A.L.-A. performed and analyzed chip-based experiments. R.S.-P., T.R., and E.R.-G. performed RNA-seq experiments and data analysis. C.G., A.L.-A., T.R., and M.M.E.-B. analyzed the results and wrote the manuscript, and prepared the figures. All authors reviewed and approved the final manuscript.

Acknowledgement

The authors wish to thank the Aragon Health System Biobank (BSSA) for providing the resources. Authors would like to acknowledge the use of Servicios Científico Técnicos del CIBA (IACS-Universidad

de Zaragoza) for their valuable technical support.

Data Availability

RNA sequencing data generated in this study are being deposited in the Gene Expression Omnibus (GEO) repository. The submission process has been initiated and metadata files have been completed. Accession numbers will be provided upon completion of the upload and prior to publication.

References

1. Hewitt, R. E. Biobanking: the foundation of personalized medicine. Curr Opin Oncol [Internet]. ;23(1). (2011). Available from: https://journals.lww.com/co-oncology/fulltext/2011/01000/biobanking__the_foundation_of_personalized.19.aspx
2. Hewitt, R. & Watson, P. Defining Biobank. *Biopreservation Biobanking*. **11** (5), 309–315. 10.1089/bio.2013.0042 (2013).
3. Corrò, C., Novellasdemunt, L. & Li, V. S. W. A brief history of organoids. *Am. J. Physiol-Cell Physiol.* **319** (1), C151–C165. 10.1152/ajpcell.00120.2020 (2020).
4. Restivo, G. et al. Live slow-frozen human tumor tissues viable for 2D, 3D, ex vivo cultures and single-cell RNAseq. *Commun. Biol.* **5** (1), 1144. 10.1038/s42003-022-04025-0 (2022).
5. Miranda, L. et al. Breast Cancer Tissues and Organoids BioBank: Constitution, Research Activities and Samples Access. *Organoids* **4** (1), 5. 10.3390/organoids4010005 (2025).
6. Tuveson, D. & Clevers, H. Cancer modeling meets human organoid technology. *Science* **364** (6444), 952–955. 10.1126/science.aaw6985 (2019).
7. Tsai, Y. H. et al. A Method for Cryogenic Preservation of Human Biopsy Specimens and Subsequent Organoid Culture. *Cell. Mol. Gastroenterol. Hepatol.* **6** (2), 218–222e7. 10.1016/j.jcmgh.2018.04.008 (2018).
8. He, A. et al. Cryopreservation of Viable Human Tissues: Renewable Resource for Viable Tissue, Cell Lines, and Organoid Development. *Biopreservation Biobanking*. **18** (3), 222–227. 10.1089/bio.2019.0062 (2020).
9. Walsh, A. J., Cook, R. S., Sanders, M. E., Arteaga, C. L. & Skala, M. C. Drug response in organoids generated from frozen primary tumor tissues. *Sci. Rep.* **6** (1), 18889. 10.1038/srep18889 (2016).
10. Chen, P. et al. Establishing a cryopreserved biobank of living tumor tissues for drug sensitivity testing. *Bioact Mater.* **46**, 582–596. 10.1016/j.bioactmat.2024.09.008 (2025).
11. Lancaster, M. A. & Knoblich, J. A. Organogenesis in a dish: Modeling development and disease using organoid technologies. *Science* **345** (6194), 1247125. 10.1126/science.1247125 (2014).
12. Kim, J., Koo, B. K. & Knoblich, J. A. Human organoids: model systems for human biology and medicine. *Nat. Rev. Mol. Cell. Biol.* **21** (10), 571–584. 10.1038/s41580-020-0259-3 (2020).

13. Yousef Yengej, F. A., Jansen, J., Rookmaaker, M. B., Verhaar, M. C. & Clevers, H. Kidney Organoids and Tubuloids. *Cells* **9** (6). 10.3390/cells9061326 (2020).
14. Takasato, M. et al. Kidney organoids from human iPS cells contain multiple lineages and model human nephrogenesis. *Nature* **526** (7574), 564–568. 10.1038/nature15695 (2015).
15. Garreta, E. et al. Systematic production of human kidney organoids for transplantation in porcine kidneys during ex vivo machine perfusion. *Nat. Biomed. Eng.* 31. 10.1038/s41551-025-01542-1 (2025 Oct).
16. Kumar, S. V. et al. Kidney micro-organoids in suspension culture as a scalable source of human pluripotent stem cell-derived kidney cells. *Development* **146** (5), dev172361. 10.1242/dev.172361 (2019).
17. Bunney, P. E., Zink, A. N., Holm, A. A., Billington, C. J. & Kotz, C. M. Orexin activation counteracts decreases in nonexercise activity thermogenesis (NEAT) caused by high-fat diet. *Physiol. Behav.* **176**, 139–148. 10.1016/j.physbeh.2017.03.040 (2017).
18. Schutgens, F. et al. Tubuloids derived from human adult kidney and urine for personalized disease modeling. *Nat. Biotechnol.* **37** (3), 303–313. 10.1038/s41587-019-0048-8 (2019).
19. Calandrini, C. et al. An organoid biobank for childhood kidney cancers that captures disease and tissue heterogeneity. *Nat. Commun.* **11** (1), 1310. 10.1038/s41467-020-15155-6 (2020).
20. Walsh, A. J., Cook, R. S., Sanders, M. E., Arteaga, C. L. & Skala, M. C. Drug response in organoids generated from frozen primary tumor tissues. *Sci. Rep.* **6** (1), 18889. 10.1038/srep18889 (2016).
21. Khoshdel-Rad, N., Ahmadi, A. & Moghadasali, R. Kidney organoids: current knowledge and future directions. *Cell. Tissue Res.* **387** (2), 207–224. 10.1007/s00441-021-03565-x (2022).
22. Freedman, B. S. Physiology assays in human kidney organoids. *Am. J. Physiol-Ren Physiol.* **322** (6), F625–F638. 10.1152/ajprenal.00400.2021 (2022).
23. Miranda, L. et al. Breast Cancer Tissues and Organoids BioBank: Constitution, Research Activities and Samples Access. *Organoids* **4** (1), 5. 10.3390/organoids4010005 (2025).
24. Gubala, J. et al. Generation and maintenance of kidney and kidney cancer organoids from patient-derived material for drug development and precision oncology. *Mol. Ther. - Methods Clin. Dev.* **32** (4), 101368. 10.1016/j.omtm.2024.101368 (2024).
25. Lacueva-Aparicio, A., Martínez-Gimeno, L., Torcal, P., Ochoa, I. & Giménez, I. Advanced Kidney Models In Vitro Using the Established Cell Line Renal Proximal Tubular Epithelial/Telomerase Reverse Transcriptase1 for Nephrotoxicity Assays. *Biomimetics* **9** (7), 446. 10.3390/biomimetics9070446 (2024).
26. Chen, E. Y. et al. Enrichr: interactive and collaborative HTML5 gene list enrichment analysis tool. *BMC Bioinform.* **14** (1), 128. 10.1186/1471-2105-14-128 (2013).
27. Kuleshov, M. V. et al. Enrichr: a comprehensive gene set enrichment analysis web server 2016 update. *Nucleic Acids Res.* **44** (W1), W90–W97. 10.1093/nar/gkw377 (2016).

28. Xie, Z. et al. Gene Set Knowledge Discovery with Enrichr. *Curr. Protoc.* **1** (3), e90. 10.1002/cpz1.90 (2021).
29. Caspers, T., Boor, P. & Klinkhammer, B. M. The roles of Tenascin C in kidney diseases. *Am. J. Physiol-Cell Physiol.* **330** (2), C552–C569. 10.1152/ajpcell.00514.2025 (2026).
30. Deng, L., Yan, F., Feng, C. & Yang, Q. Multi-Omics Analysis and Nephroseq Database of Genes Related to Kidney Function in Diabetic Nephropathy Patients to Predict Potential Target Drugs. *Diabetes Metab. Syndr. Obes.* **18**, 3781–3794. 10.2147/DMSO.S526696 (2025).
31. Wang, Y. et al. Proximal tubule-derived colony stimulating factor-1 mediates polarization of renal macrophages and dendritic cells, and recovery in acute kidney injury. *Kidney Int.* **88** (6), 1274–1282. 10.1038/ki.2015.295 (2015).
32. Edwards, M., Blanquie, O., Moriarty, O., Beken, S. & Ehmann, F. New approach methodologies: EU regulatory horizons. *Nat. Rev. Drug Discov*. **24** (8). 10.1038/d41573-025-00053-7 (2025). PubMed PMID: 40128617.
33. Svendsen, C. N. Adopting novel alternative methods (NAMs) for biomedical research—What is the right approach? *Cell. Stem Cell.* **32** (10), 1489–1490. 10.1016/j.stem.2025.08.014 (2025).
34. Hope, L. & Bailey, J. Breaking down the barriers to animal-free research. *Altern. Lab. Anim.* **53** (4), 215–231. 10.1177/02611929251349465 (2025).
35. Huang, B. et al. Spatially patterned kidney assembloids recapitulate progenitor self-assembly and enable high-fidelity in vivo disease modeling. *Cell. Stem Cell.* **32** (10), 1614–1633e13. 10.1016/j.stem.2025.08.013 (2025).
36. Kearney, H., Mihăilă, S. M., Moroni, L. & Mota, C. Kidney Organoids in Drug Development: Integrating Technological Advances and Standardization for Effective Implementation. *Adv. Healthc. Mater.* e04719. 10.1002/adhm.202504719 (2025).
37. Li, Z. et al. Patient-derived renal cell carcinoma organoids for personalized cancer therapy. *Clin. Transl Med.* **12** (7), e970. 10.1002/ctm2.970 (2022).
38. Nunez-Nescolarde, A. B. et al. Comparative Analysis of Human Kidney Organoid and Tubuloid Models. *Kidney360* **6** (7), 1073–1084. 10.34067/KID.0000000834 (2025).
39. He, A. et al. Cryopreservation of Viable Human Tissues: Renewable Resource for Viable Tissue, Cell Lines, and Organoid Development. *Biopreservation Biobanking*. **18** (3), 222–227. 10.1089/bio.2019.0062 (2020).
40. Walsh, A. J., Cook, R. S., Sanders, M. E., Arteaga, C. L. & Skala, M. C. Drug response in organoids generated from frozen primary tumor tissues. *Sci. Rep.* **6** (1), 18889. 10.1038/srep18889 (2016).
41. Kusaba, T., Lalli, M., Kramann, R., Kobayashi, A. & Humphreys, B. D. Differentiated kidney epithelial cells repair injured proximal tubule. *Proc. Natl. Acad. Sci.* **111** (4), 1527–1532. 10.1073/pnas.1310653110 (2014).
42. Li, Z. L. et al. Renal tubular epithelial cells response to injury in acute kidney injury. *eBioMedicine* **107**, 105294. 10.1016/j.ebiom.2024.105294 (2024).

43. Mashouf, P., Tabibzadeh, N., Kuraoka, S., Oishi, H. & Morizane, R. Cryopreservation of human kidney organoids. *Cell. Mol. Life Sci.* **81** (1), 306. 10.1007/s00018-024-05352-7 (2024).
44. Nishimura, Y. Vascularization and maturation of kidney organoids: a comprehensive review of technological trends and challenges. *J. Artif. Organs*. **29** (1), 18. 10.1007/s10047-026-01545-y (2026).
45. Morizane, R. et al. Nephron organoids derived from human pluripotent stem cells model kidney development and injury. *Nat. Biotechnol.* **33** (11), 1193–1200. 10.1038/nbt.3392 (2015).
46. Morizane, R. & Bonventre, J. V. Generation of nephron progenitor cells and kidney organoids from human pluripotent stem cells. *Nat. Protoc.* **12** (1), 195–207. 10.1038/nprot.2016.170 (2017).
47. Forbes, T. A. et al. Patient-iPSC-Derived Kidney Organoids Show Functional Validation of a Ciliopathic Renal Phenotype and Reveal Underlying Pathogenetic Mechanisms. *Am. J. Hum. Genet.* **102** (5), 816–831. 10.1016/j.ajhg.2018.03.014 (2018).
48. Yamaguchi, S. et al. Generation of kidney tubular organoids from human pluripotent stem cells. *Sci. Rep.* **6** (1), 38353. 10.1038/srep38353 (2016).
49. van den Berg, C. W. et al. Renal Subcapsular Transplantation of PSC-Derived Kidney Organoids Induces Neo-vasculogenesis and Significant Glomerular and Tubular Maturation In Vivo. *Stem Cell. Rep.* **10** (3), 751–765. 10.1016/j.stemcr.2018.01.041 (2018).
50. Aceves, J. O. et al. 3D proximal tubule-on-chip model derived from kidney organoids with improved drug uptake. *Sci. Rep.* **12** (1), 14997. 10.1038/s41598-022-19293-3 (2022).
51. Hiratsuka, K. et al. Organoid-on-a-chip model of human ARPKD reveals mechanosensing pathomechanisms for drug discovery. *Sci. Adv.* **8**(38):eabq0866. 10.1126/sciadv.abq0866
52. Homan, K. A. et al. Flow-enhanced vascularization and maturation of kidney organoids in vitro. *Nat. Methods*. **16** (3), 255–262. 10.1038/s41592-019-0325-y (2019).
53. Monteduro, A. G. et al. Organs-on-chips technologies – A guide from disease models to opportunities for drug development. *Biosens. Bioelectron.* **231**, 115271. 10.1016/j.bios.2023.115271 (2023).
54. Musah, S., Bhattacharya, R. & Himmelfarb, J. Kidney Disease Modeling with Organoids and Organs-on-Chips. *Annu. Rev. Biomed. Eng.* **26** (1), 383–414. 10.1146/annurev-bioeng-072623-044010 (2024).
55. Gijzen, L. et al. Culture and analysis of kidney tubuloids and perfused tubuloid cells-on-a-chip. *Nat. Protoc.* **16** (4), 2023–2050. 10.1038/s41596-020-00479-w (2021).
56. Bernardi, M. D. L. et al. A Novel Human Distal Tubuloid-on-a-Chip Model for Investigating Sodium and Water Transport Mechanisms [Internet]. Bioengineering; [cited 2026 May 18]. Available from: http://biorxiv.org/lookup/doi/ (2025). 10.1101/2025.03.27.644139 doi:10.1101/2025.03.27.644139.
57. Nguyen, V. V. T. et al. A human kidney and liver organoid-based multi-organ-on-a-chip model to study the therapeutic effects and biodistribution of mesenchymal stromal cell-derived extracellular vesicles. *J. Extracell. Vesicles*. **11** (11), 12280. 10.1002/jev2.12280 (2022).

Figures

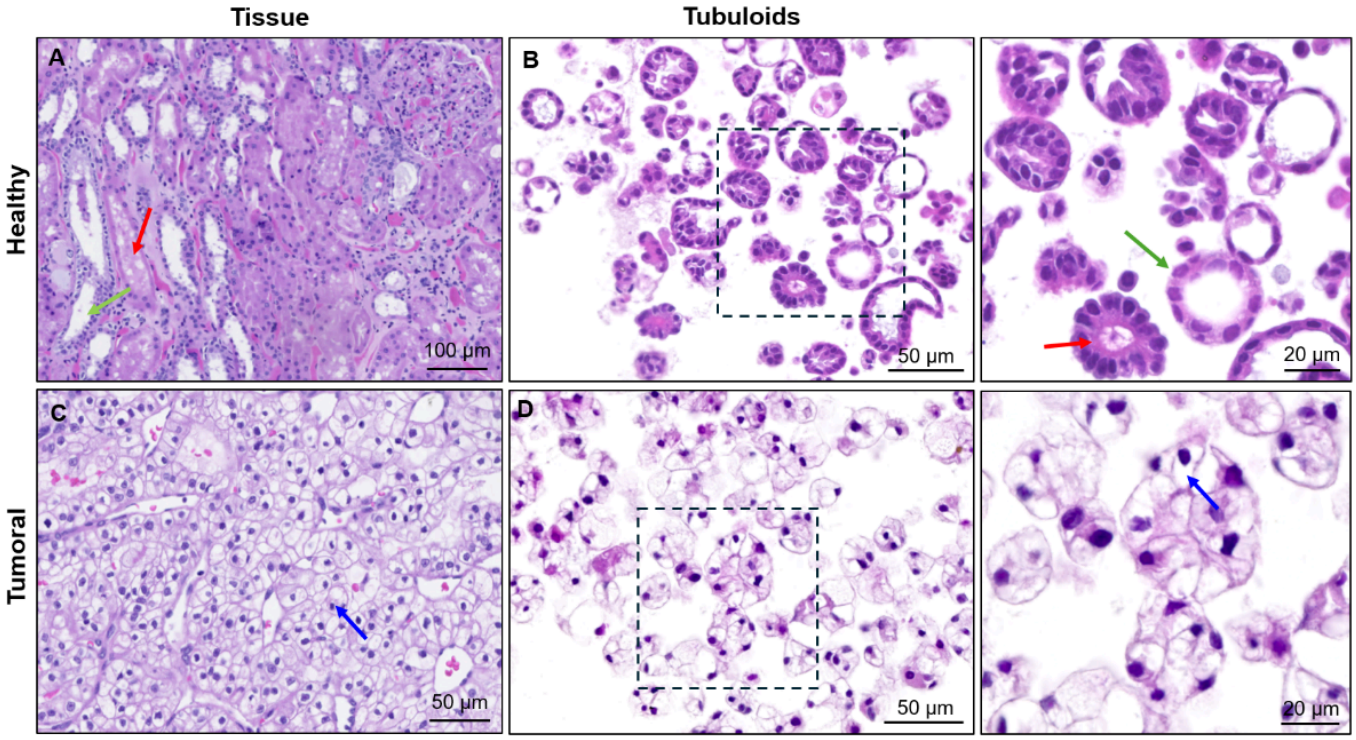


Figure 1

Tubuloids presented structures found in the original tissue. Tubuloids derived from healthy tissue (B) recapitulated estructures that resembled proximal (red arrow) and distal (green arrow) tubules when compared with the tissue from they were generated (A). Tumor-derived tubuloids (D) also resembled the original structures from the tumoral tissue which corresponds to clear cell renal cell carcinoma (blue arrow) (ccRCC) (C). Hematoxylin and eosin staining.

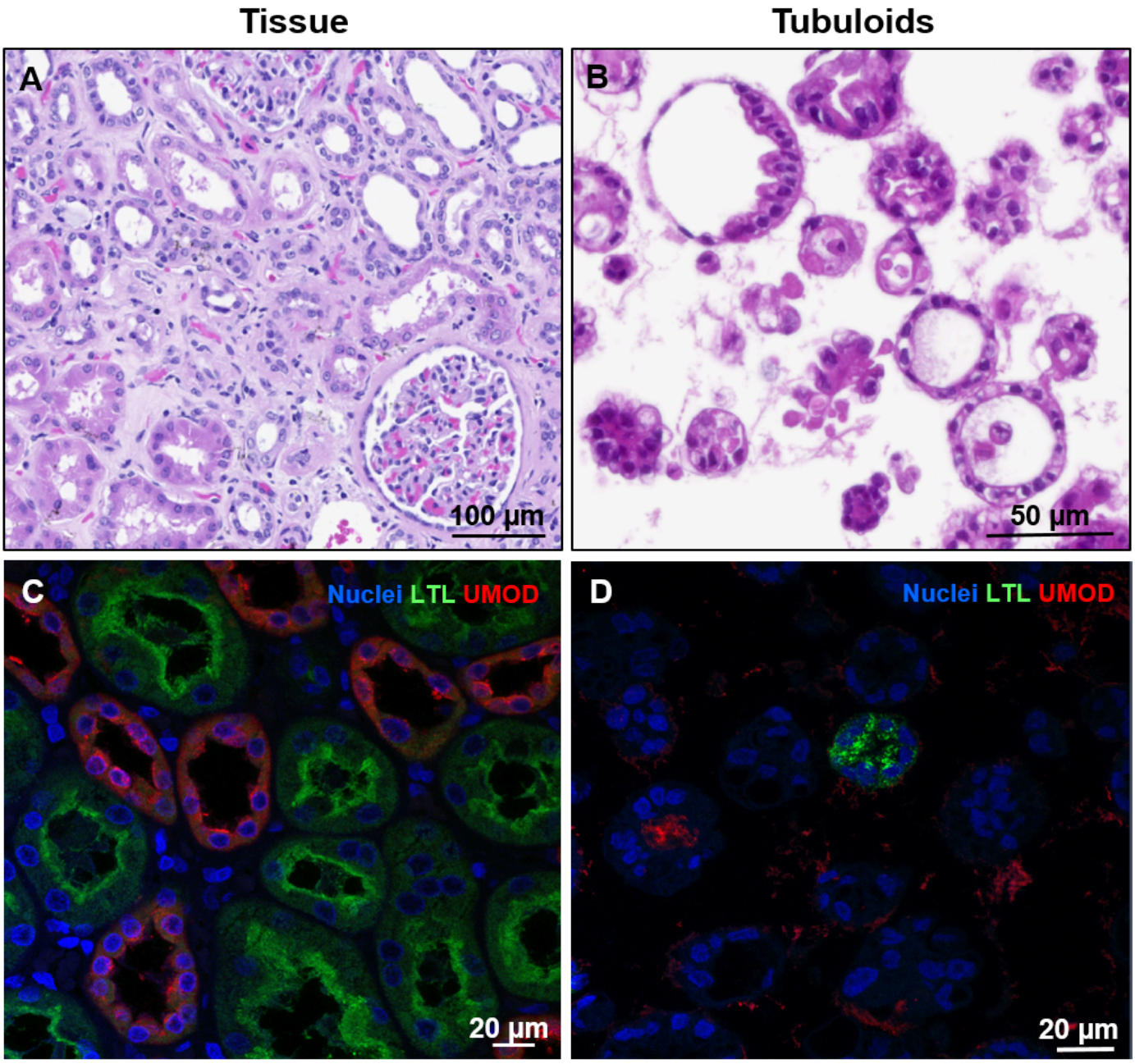


Figure 2

Specific markers from different parts of the nephron were observed by immunostaining.

Hematoxylin and eosin staining was performed to confirm the preservation of the different cell types present in the tubular compartment of the nephron, including the proximal and distal tubules (A,B). LTL (green) expression was observed both in the original healthy tissue and in the tubuloids derived from that tissue, labeling proximal tubule cells. UMOD (red), which is expressed in the distal tubule of the nephron, was also detected in both the tissue of origin and the corresponding tubuloids. Nuclei (blue). Scale bar 20 µm (C,D).

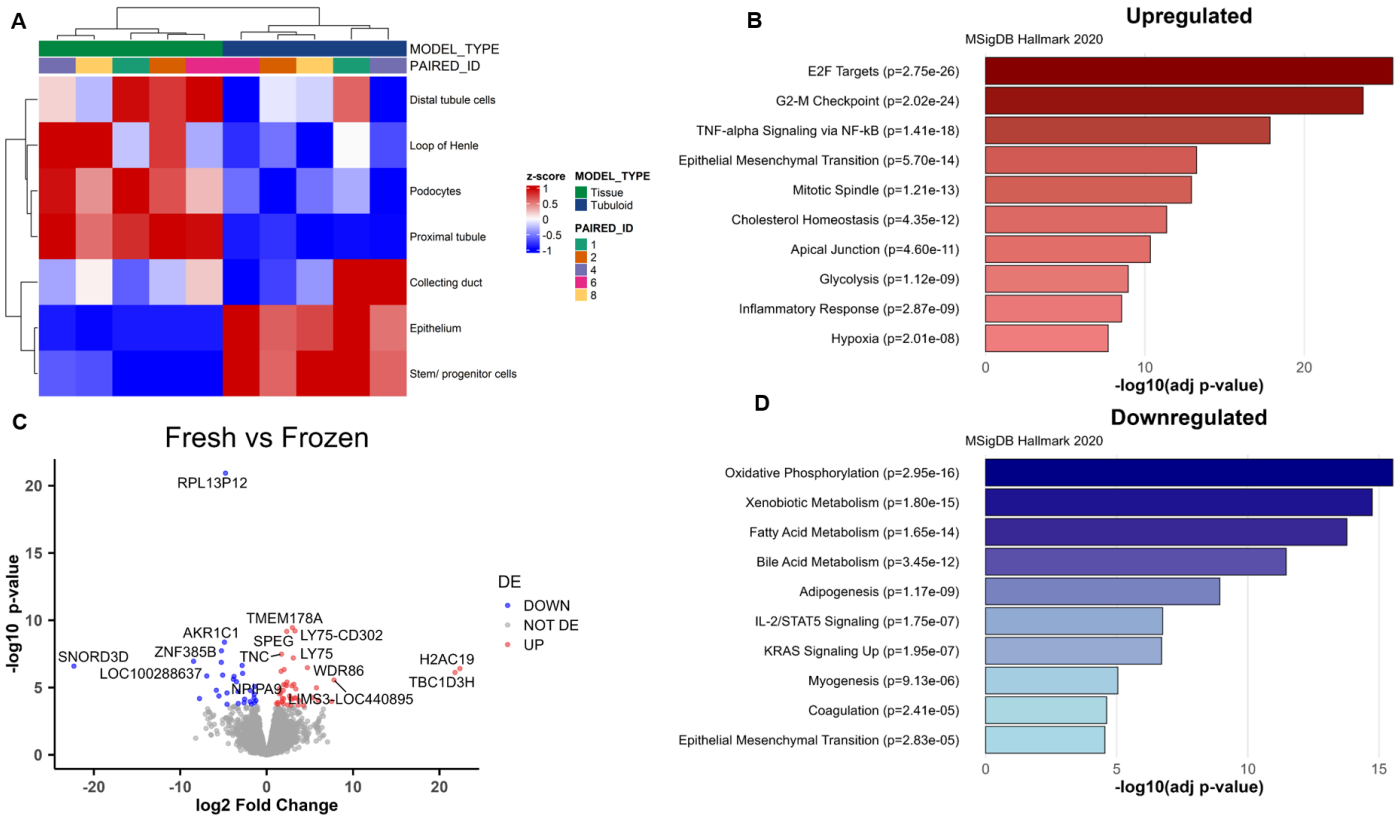


Figure 3

Transcriptomic analysis of normal tubuloids. Heat map showing the expression of cell-specific markers in native tissue and tubuloids (A). Significantly enriched pathways in tubuloids (B). Volcano plot showing differential expression in tubuloids derived from fresh and frozen tissue (C).

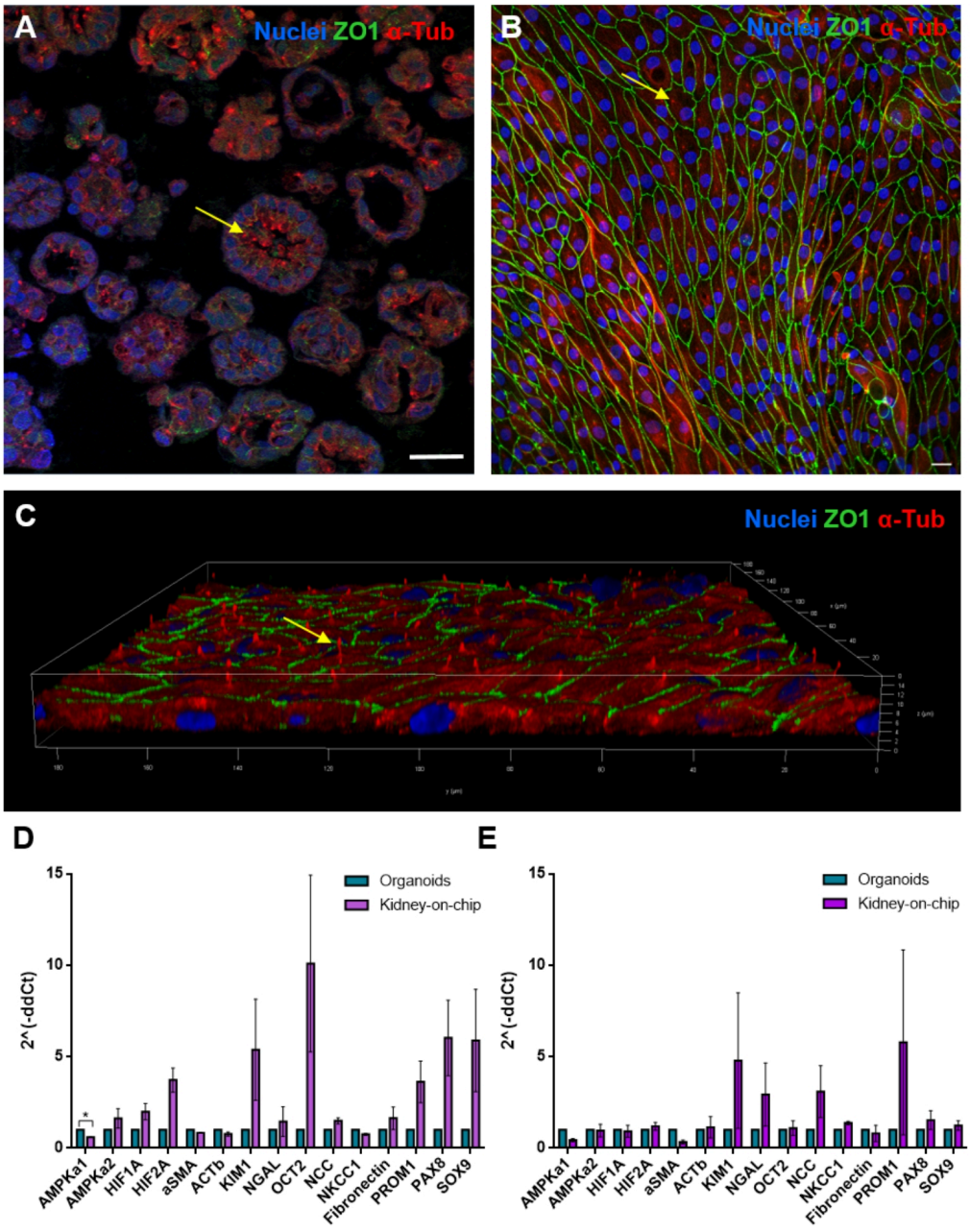


Figure 4

Microfluidic device culture. Tubuloids and cell culture monolayer in the microfluidic device showed cell polarization towards the lumen. Both tubuloids (A) and kidney-on-chip derived from these tubuloids showed ZO1 and alpha-Tubulin expression, with the primary cilium projecting to the lumen (yellow arrows). Scale bar 20 um. Expression of different markers were analyzed by qPCR comparing the tubuloids with the kidney-on-chip models from two different patient samples (D,E). Results showed

variability between samples and no statistically significant differences were found in any of the markers except for AMPKa1. Nuclei (blue), ZO-1 (green), α-tubulin (red).

Supplementary Files

This is a list of supplementary files associated with this preprint. Click to download.

- SupplementaryInformation.docx